Surface Moisture and Vegetation Cover Analysis for Drought Monitoring in the Southern Kruger National Park Using Sentinel-1, Sentinel-2, and Landsat-8

Marcel Urban [1],*, Christian Berger [1], Tami E. Mudau [2], Kai Heckel [1], John Truckenbrodt [1], Victor Onyango Odipo [1], Izak P. J. Smit [3,4] and Christiane Schmullius [1]

[1] Department for Earth Observation, Institute of Geography, Friedrich-Schiller-University Jena, Loebdergraben 32, 07743 Jena, Germany; christian.berger@uni-jena.de (C.B.); kai.heckel@uni-jena.de (K.H.); john.truckenbrodt@uni-jena.de (J.T.); victor.onyango@uni-jena.de (V.O.O.); c.schmullius@uni-jena.de (C.S.)

[2] CSIR (Council for Scientific and Industrial Research), Meiring Naudé Road, Brummeria, Pretoria 0184, South Africa; saicon@csir.co.za

[3] Scientific Services, South African National Parks, Private Bag X402, Skukuza 1350, South Africa; izak.smit@sanparks.org

[4] Centre for African Ecology, School of Animal, Plant and Environmental Sciences, University of the Witwatersrand, Private Bag 3, Wits 2050, South Africa

* Correspondence: marcel.urban@uni-jena.de; Tel.: +49-3641-9-48887

check for updates

Abstract: During the southern summer season of 2015 and 2016, South Africa experienced one of the most severe meteorological droughts since the start of climate recording, due to an exceptionally strong El Niño event. To investigate spatiotemporal dynamics of surface moisture and vegetation structure, data from ESA's Copernicus Sentinel-1/-2 and NASA's Landsat-8 for the period between March 2015 and November 2017 were utilized. In combination, these radar and optical satellite systems provide promising data with high spatial and temporal resolution. Sentinel-1 C-band data was exploited to derive surface moisture based on a hyper-temporal co-polarized (vertical-vertical—VV) radar backscatter change detection approach, describing dynamics between dry and wet seasons. Vegetation information from a TLS (Terrestrial Laser Scanner)-derived canopy height model (CHM), as well as the normalized difference vegetation index (NDVI) from Sentinel-2 and Landsat-8, were utilized to analyze vegetation structure types and dynamics with respect to the surface moisture index (SurfMI). Our results indicate that our combined radar–optical approach allows for a separation and retrieval of surface moisture conditions suitable for drought monitoring. Moreover, we conclude that it is crucial for the development of a drought monitoring system for savanna ecosystems to integrate land cover and vegetation information for analyzing surface moisture dynamics derived from Earth observation time series.

Keywords: drought monitoring; surface moisture; time series analysis; savanna ecosystems; Sentinel-1; NDVI; Sentinel-2; Landsat-8; Kruger National Park

1. Introduction

South Africa has faced one of the most severe meteorological droughts during the southern summer season of 2015 and 2016, due to an exceptional El Niño event, which was ranked as third strongest since climate recordings [1,2]. The El Niño/Southern Oscillation phenomenon (ENSO), which is driven by fluctuations of ocean temperatures in the equatorial Pacific [3], is negatively correlated with the amount of rainfall during the summer season in southern Africa [4,5]. Thus, a strong ENSO phenomenon has enormous impacts on ecosystem dynamics, as well as agricultural and biomass productivity in

semiarid regions of southern Africa [6,7]. The classification of ENSO is challenging, as the phenomenon varied in strength and duration throughout the last century [8].

During the summer season 2015/2016, ENSO has caused a delay in the start of rainfall as well as a decrease of the total amount of precipitation in the summer rainfall areas of South Africa causing a meteorological drought, with exceptional impacts to the northeastern region, including the Kruger National Park (KNP) (Figure 1). Although droughts are natural phenomena and have important ecological roles to play in natural settings, they often result in suffering and the loss of human livelihoods, and have various negative environmental and economic impacts, especially in the agricultural sector. Compared on a continental level, Africa in particular has faced the majority of drought events (up to 300) throughout the last century, with increasing trends in frequency, strength, and spatial extent [9]. However, each drought is unique, and differs in intensity and duration [10]. In 2015/2016, a particularly severe drought had extensive consequences for several million people by threatening the food security and causing the outbreak of diseases and decline in medical care [1,2].
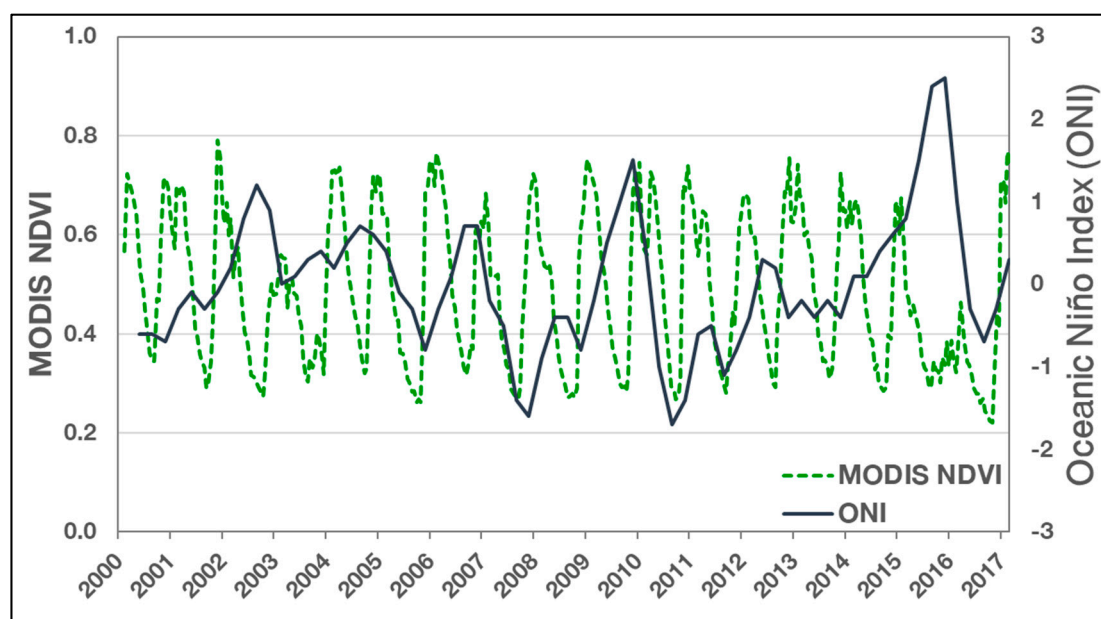

Figure 1. Moderate-Resolution Imaging Spectroradiometer (MODIS)-normalized difference vegetation index (NDVI) time series of the area (10 km × 10 km) around the Skukuza flux tower (25°1.184′S, 31°29.813′E) and the oceanic Niño index (ONI) [11,12]. Note the significant decrease in NDVI during the meteorological drought of 2015/2016 in combination with the occurrence of an extreme El Niño event.

Particularly the savanna ecosystems, which are covering 20% of the global terrestrial surface [13] and nearly 50% of Africa, are ecologically and economically of high importance [14], and have many humans directly dependent on them. The savanna ecosystems in South Africa, which are characterized by woody plants (e.g., shrubs and trees) and grasslands with seasonal changes due to dry and wet seasons, are vulnerable to impacts from droughts, fires, herbivory, etc. [13,15,16]. High spatial resolution time series information on vegetation structure, as well as moisture properties of the surface, are important parameters to analyze these impacts [17,18]. The monitoring of changes in vegetation structure and dynamics, which are influenced by external factors (e.g., droughts, fires, herbivory, etc.) is one of the essential components for the management of the Kruger National Park [19].

Various studies focused on the development of drought monitoring concepts using Earth observation data from different sources [20] for different applications, such as agriculture [21,22], grasslands [23,24], as well as savanna ecosystems [25,26]. So far, the majority of these studies have used optical remote sensing information with coarse spatial resolution (e.g., MODIS (Moderate-Resolution Imaging Spectroradiometer), AVHRR (Advanced Very High Resolution Radiometer)) for analyzing

drought indicators such as the NDVI (normalized difference vegetation index), EVI (enhanced vegetation index), VCI (vegetation condition index), as well as the SPI (standard precipitation index) [26]. However, additional parameters derived from microwave remote sensing data, surface moisture in particular, are essential in the analysis and monitoring of impacts and dynamics of droughts in various ecosystems [20]. The retrieval of surface moisture information for analyzing the impacts of droughts is of high importance, as it is highly correlated to vegetation and soil respiration, which represents both root and microbial respiration, and is one of the main fluxes of carbon in savanna ecosystems [27].

Earth observation-based soil moisture missions, such as SMOS (soil moisture and ocean salinity) and SMAP (soil moisture active passive) are using L-band microwave techniques for the retrieval of global soil moisture information with coarse spatial resolution (around 50 km) [28,29]. During recent years, various studies were carried out utilizing C-band SAR (Synthetic Aperture Radar) data, from e.g., ERS-1/2 (European Remote Sensing) [30–32], ENVISAT ASAR (Environmental Satellite—Advanced Synthetic Aperture Radar) [33–35], as well as RADARSAT [36–38], in various observation modes for soil moisture applications on different scales. The new Sentinel-1 C-band SAR, with high spatial resolution and repetition rate, offers new perspectives in the retrieval of surface moisture information with C-band SAR [39]. The potential of surface moisture retrieval using Sentinel-1 C-band data have already been tested during the pre-launch phase [40,41]. Compared to other surface moisture approaches from different Earth observation data sources [42,43] and hydrological approaches [44,45], Sentinel-1 data has, so far, only been used in a few studies for surface moisture mapping. Gao et al. [46] have been analyzing the synergistic usage of Sentinel-1 and Sentinel-2 for surface moisture mapping at coarse spatial scale (100 m).

The potential for analyzing surface moisture in savanna ecosystems retrieved from spatial and temporal high-resolution Sentinel-1 time series, in combination with vegetation information from Sentinel-2 and Landsat-8, has not been addressed, so far, in the literature. The increasing availability of Earth observation data introduces new challenges in developing synergistic approaches utilizing optical and microwave satellite information (e.g., Sentinel-1/-2, Landsat-8) for drought monitoring with high spatial and temporal resolution [20]. The launch of recent satellite missions, such as the Sentinel fleet of ESA's Copernicus programme and Landsat-8, has led to a tremendous increase in the available Earth observation data provided without cost, increasing the potential for the synergetic usage of optical and radar data suitable for drought monitoring. The increase in data availability creates new opportunities for analyzing data not only in the spatial but also temporal domain, by using time series visualizing processes on the Earth's surface, e.g., surface moisture dynamics.

The overall goal of this study is to analyze the potential of deriving surface moisture and vegetation information for drought monitoring in the savanna ecosystem of the southern part of the KNP using Sentinel-1, Sentinel-2, and Landsat-8 time series. The region of interest is the area around the Skukuza flux tower, which is situated close to the main tourist rest camp of Skukuza, where the administrative headquarter of the KNP is located. By applying a change detection technique [47,48] to VV-polarized Sentinel-1 C-band GRD (ground range detected) backscatter time series, it was possible to derive a surface moisture index (SurfMI) capturing the dynamics within the study area at a high spatial (10 m pixel size) and temporal resolution. The radar-based surface moisture information was compared to in situ soil moisture data from two probes, as well as precipitation measurements from two climate stations located in the study area. In addition, vegetation classes extracted from a TLS (Terrestrial Laser Scanner) height information dataset have been used to analyze moisture dynamics for different land cover units on small scale. Using NDVI information derived from Sentinel-2 and Landsat-8 time series, it was possible to analyze the impact of surface moisture changes to different land cover classes by using image object segmentation.

2. Study Area

The study area is located in the southern KNP, South Africa (Figure 2). The focus region is situated approximately 13 km southwest of Skukuza, and covers an area of about 50 km² around the

eddy covariance flux tower, built in 2000. It is part of the study area of the Adaptive Resilience of Southern African Ecosystems (ARS AfricaE) research project [13], where the tower is used to analyze biogeochemical interactions and their significance to the resilience of the savanna ecosystem to climate change [49].

The elevation of the region is around 365 m a.s.l. and is formed by the N'waswitshaka catchment, which is nested within the larger catchment of the perennial Sabie River. The area is classified as broad- and fine-leafed savanna, with the dominant tree species belonging to the *Combretum* and *Acacia* genera. The wet season starts end of October and lasts until end of April, with a mean annual precipitation of around 550 mm, with large interannual variability [50]. The temperature varies between mild in winter, with July being the coldest month in Skukuza (average minimum 5.6 °C; average maximum 25.9 °C), to hot in summer, with January the hottest month (average minimum 20.6 °C; average maximum 32.6 °C) [51].
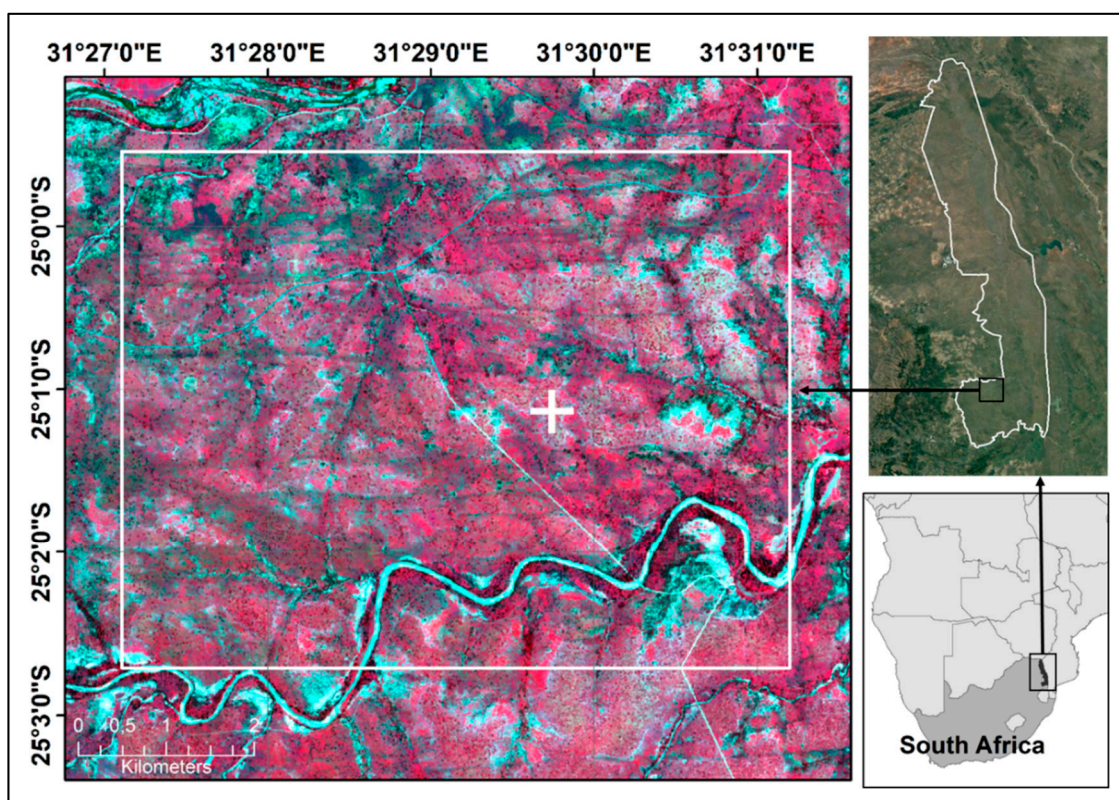

Figure 2. Location of the study area (ca. 50 km^2) in the southern Kruger National Park (KNP) (Skukuza eddy covariance flux tower and in situ soil moisture probes, white cross) (Imagery source: Copernicus Sentinel-2A data 19 January 2017 (R: Band 8; G: Band 4; B: Band 3)/Google Earth/FAO Country Shape).

3. Materials and Methods

3.1. Materials

Recent satellite missions from ESA's Copernicus programme and Landsat Data Continuity Mission (LDCM) has led to an enormous increase in available Earth observation data. This introduces new opportunities for analyzing data with higher spatial and temporal resolution for different applications, e.g., drought monitoring. With the new ESA SAR satellite Sentinel-1A, there is now the possibility to observe the Earth's surface with a repeat rate of up to twelve days and a spatial resolution of 10 m regardless of atmospheric effects and sun illumination. In combination with Sentinel-1B, the temporal resolution would increase up to less than six days, depending on the geographic location.

However, data from Sentinel-1B have not been utilized in this study, as it has been operated since October 2016 only. The study site data coverage for the three satellites used in this study is shown in Figure 3.
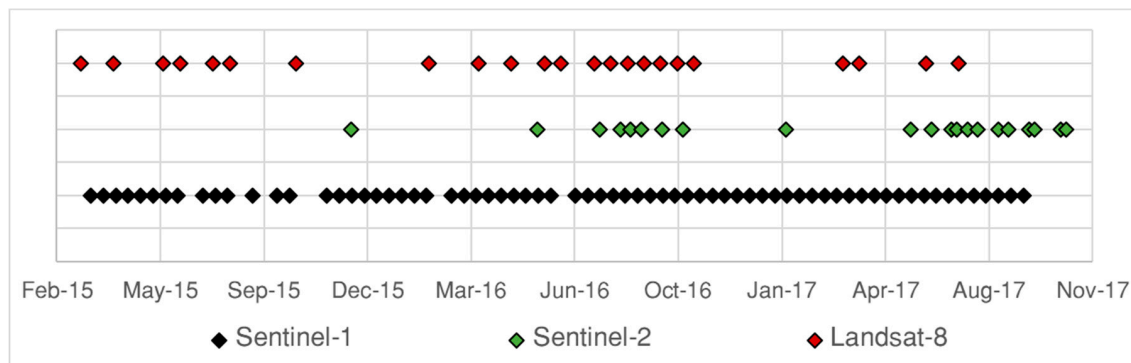

Figure 3. Overview of the temporal data coverage of 69 Sentinel-1A, 21 Sentinel-2A/-2B, and 23 Landsat-8 satellite scenes.

3.1.1. Sentinel-1 Data and Pre-Processing

The analysis of the C-band Sentinel-1A surface moisture time series was done using 69 scenes acquired between 20 March 2015 and 5 September 2017 in GRD Mode from relative orbit 145, which covers the entire KNP extent. With some smaller gaps in this time series, the used Sentinel-1A data have an average repeat cycle of 12 days (see Figure 3).

The pre-processing of the Sentinel-1A data has been done using pyroSAR, a Python framework for large-scale SAR satellite data processing [52]. The pyroSAR environment aims to provide a complete solution for the organization and pre-processing of SAR satellite data from recent and historical satellite missions for applications on the scale of personal computers up to large server infrastructures, using various open source tools and libraries. Moreover, pyroSAR provides a user-friendly access to processing utilities in ESA's Sentinel Application Platform (SNAP), as well as GAMMA Remote Sensing software. Once the images are pre-processed, further functionalities are available for mosaicking and resampling images to common pixel boundaries suited for time series analysis.

Within pyroSAR, the Sentinel-1A data, with a spatial resolution of 10 m, have been pre-processed using GAMMA (Software Version: December 2016, GAMMA Remote Sensing AG, 3073 Gümligen, Switzerland) [53]. In a first step, each individual scene was radiometrically calibrated. Besides using the precise orbit state vectors (precise orbit ephemerides), height information from the SRTM (Shuttle Radar Topographic Mission) (30 m) was utilized for the orthorectification of the data [54]. Furthermore, terrain flattening of the data, whereby the backscatter values are converted from beta naught (β^0) to gamma naught (γ^0), was performed for which the SRTM data was also used [55].

3.1.2. Optical Earth Observation Data

Sentinel-2 Imagery

The Sentinel-2A/-2B images (Tile No.: 36JUT) used for this study were retrieved via the Copernicus Open Access Hub (https://scihub.copernicus.eu/). In total, 21 cloud free satellite scenes covering a period from 26 November 2015 to 16 October 2017 have been identified and downloaded (Figure 3). As the Sentinel-2 data are delivered at Level 1C (orthorectified top of atmosphere (TOA) reflectance), an atmospheric correction was applied using Sen2Cor (Version 2.5.0) [56], which is embedded in ESA's SNAP software. Sen2Cor uses a cloud detection algorithm and detects both aerosol optical thickness and water vapor. Various parameters, such as terrain correction, definition of aerosol type, ozone, etc., have been set within Sen2Cor before converting TOA to surface reflectance values [56].

Landsat-8 Imagery

Although Sentinel-2 images are covering the study area, cloud free acquisitions were only available after the 26 November 2015. Thus, we incorporated satellite information from Landsat-8 (Path 168/Row 77) in order to increase the data availability of optical satellite information for this study. We identified 23 Landsat-8 scenes in total, covering the period between 10 March 2015 and 5 July 2017 (Figure 3). This enables the expansion of the time series, as well as shortening the time interval in combination with Sentinel-2.

The Landsat-8 Level-2 products were acquired via the USGS (United States Geological Survey) Earth Explorer. This platform provides ready-to-use surface reflectance Landsat data processed by the EROS (Earth Resources Observation and Science) Science Processing Architecture (ESPA) on-demand interface, the Landsat Surface Reflectance Code (LaSRC) [57].

3.1.3. In Situ Data Sources

Precipitation Records

Long-term precipitation information was available via the SANParks (South African National Park) data repository. A climate station is located in Skukuza, which is approximately 13 km in eastern direction from the central point of the study area, and measures the daily amounts of precipitation in mm [58]. Additional precipitation records from the Skukuza flux tower were made available by CSIR (Council for Scientific and Industrial Research). As the study area covers these two climate stations, both precipitation records are averaged for the following analysis.

In Situ Soil Moisture Measurements

In situ soil moisture information was available for an area near the Skukuza flux tower (25°1.184′S, 31°29.813′E). The soil moisture was measured using a CS-616 Soil Moisture Probe (Campbell Scientific Inc., Logan, UT, USA). This ground station consists of two units, which are acquiring volumetric moisture content (m^3/m^3) and the soil temperature (in °C) at 6, 13, 26, and 59 cm depth. For this study, only moisture information from the upper 6 cm was used, as there are no significant dependencies or direct influences to the radar signal below this depth [59]. The values from both probes were averaged for each time step to one single soil moisture measurement.

Terrestrial Laser Scanner Data

A high spatial resolution (0.06 m) canopy height model (CHM), which was extracted from TLS data, was utilized to detect trees, shrubs, and ground pixels around the Skukuza flux tower location. The TLS data was acquired using a RIEGL VZ-1000 (RIEGL Laser Measurement Systems GmbH, 3580 Horn, Austria) and covers a footprint of 51.8 ha. Additional information about the TLS data and the creation of the CHM can be found in Odipo et al. [60].

The pixel size of the canopy height model was rescaled to 10 m, representing the spatial resolution of the Sentinel-1A data. The rescaling process was done using the value of the 95th percentile below each pixel, which reduces the possibility of including potential outliers. We used percentile information in order to retrieve "true" tree cover pixel as well as ground pixel with no vegetation cover inside the resolution cell.

3.2. Methods

The methodological framework of this study is shown in Figure 4. In general, the workflow is based on the analysis of cross-polarized Sentinel-1 C-band GRD backscatter time series information for a change detection-based surface moisture retrieval at high spatial resolution (10 m) (see Section 3.2.1). Vegetation greenness information (NDVI) derived from Sentinel-2 and Landsat-8 time series were

used in order to analyze the impact of surface moisture changes on different land cover classes (see Section 3.2.2).
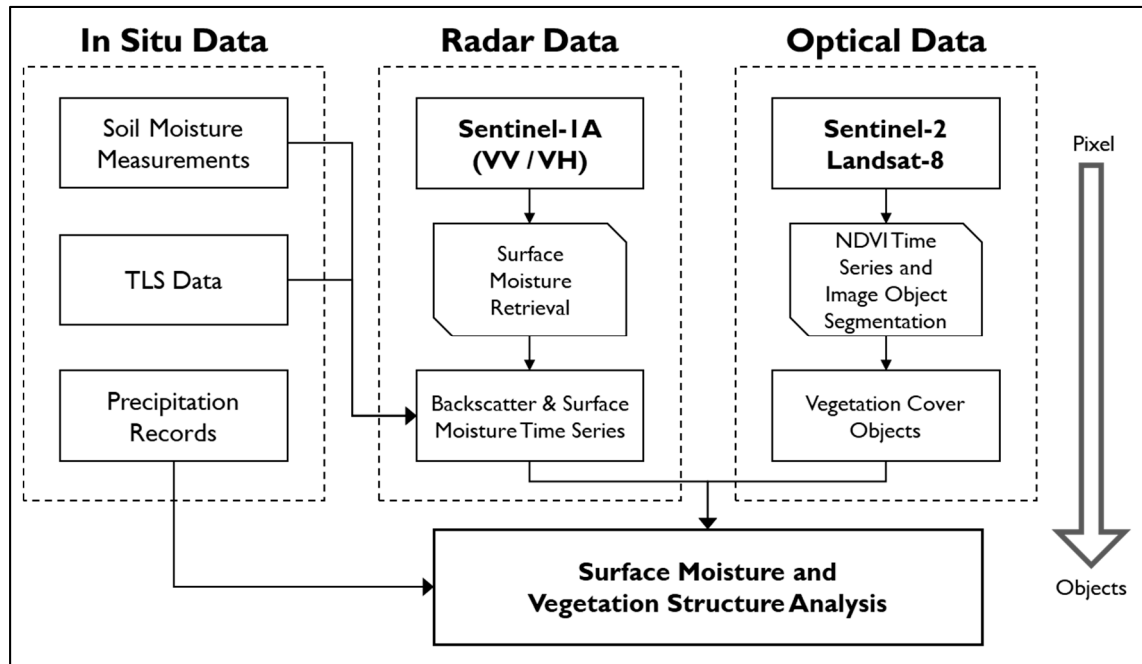

Figure 4. Methodological framework for the retrieval of a surface moisture index from radar time series, as well as vegetation information and dynamics from optical earth observation data.

3.2.1. Surface Moisture Retrieval using Sentinel-1 Time Series

The SurfMI, which was utilized as an indicator for analyzing the impact of drought in the study area, was derived using multi-temporal C-band time series information from VV-polarized Sentinel-1 data. It is assumed that factors influencing the radar backscatter signal are variable over time. Influences of vegetation and surface roughness affect long-term changes, whereas short-term variations of the backscatter are associated with moisture variations. The high temporal resolution of Sentinel-1 SAR time series is a precondition for the development of relative surface moisture ($m_s(t)$) mapping using the following equation, as shown in [47,48]:

$$m_s(t) = \frac{\sigma^0(t) - \sigma^0_{dry}(t)}{\sigma^0_{wet}(t) - \sigma^0_{dry}(t)} * 100, \tag{1}$$

where $\sigma^0(t)$ represents a pixel time series. $\sigma^0_{wet}(t)$ and $\sigma^0_{dry}(t)$ denote the minimum and maximum backscatter values observed over the study period, which are considered to be equivalent to the soil's dry reference (permanent wilting level) and wet reference (field capacity), respectively. In this study, we used the 5th percentile as dry reference, and the 95th percentile as wet reference, in order to account for outliers related to speckle noise. By applying Equation (1) to the entire time series dataset, it is possible to linearly scale the remaining SAR backscatter values between these two extremes. Values lower and higher than the defined references are set to 0 or 100, respectively. The resulting relative SurfMI, with a data range between 0% and 100%, allows for the analysis of surface moisture dynamics in order to identify the impact of droughts. Including additional soil information, such as the bulk density, would allow for a conversion from the relative index to absolute volumetric soil moisture values [61,62].

3.2.2. Differentiation of Vegetation Cover Classes

Based on the atmospheric corrected Landsat-8 and Sentinel-2 data, we calculated the NDVI (normalized difference vegetation index) [63], in order to retrieve time series information of vegetation greenness. The NDVI is calculated as the ratio of the difference between the red and near-infrared signal of the electrometric spectrum divided by the sum of both, which refers to the spectral bands 4 and 5 for Landsat-8, and bands 4 and 8 for Sentinel-2. Vegetation indices, such as the NDVI, are essential tools for monitoring savanna ecosystem functions and describing the vegetation activity as well as productivity [17]. Combining data from different satellites is challenging, as discrepancies due to different sensor properties (e.g., spectral bandwidth) might be present. Hence, the NDVI information has been corrected based on the study of [64], in order to reduce discrepancies when comparing data across satellite sensors. The NDVI time series was then used as input for calculating multi-temporal statistics, such as mean, standard deviation, percentiles, etc. An image object segmentation was carried out using eCognition Developer software (Version 9). We found that the 5th percentile and 95th percentile are most suitable to discriminate between areas characterized by different vegetation cover. Moreover, a chessboard segmentation algorithm, where each segment has the same size as the related pixel, was utilized to assign objects to different vegetation cover classes, such as closed (>60%), open (20–60%), and sparse (<20%) as defined by [65]. This was done using an NDVI threshold, which has been identified as the most suitable value to detect individual or clusters of trees or shrubs in the study area (mean NDVI > 0.4). In addition, we used this NDVI threshold to mask out trees and shrub in the class of sparse vegetation, in order to detect dynamics of bare ground as well as seasonal grass.

4. Results

4.1. Comparing Sentinel-1-Derived Surface Moisture Information to In Situ Soil Moisture Information

The Sentinel-1-derived SurfMI data was compared to the in situ soil moisture measurements of a unit located near the Skukuza flux tower. The area is characterized by bare soil and sparse vegetation. As mentioned before, only the in situ moisture information measured at a depth of 6 cm was used, as there are no dependencies or direct influences to the C-band radar signal below such depth [59].

The comparison of in situ and Sentinel-1-derived moisture was done for a 3-by-3 pixel area covering the location of the in situ soil moisture probes. The moisture values from Sentinel-1 were averaged for nine pixel for each individual time step. In addition, the two daily values of the probes were averaged and compared to the Sentinel-1-derived surface moisture information. This results in a moderate Pearson correlation coefficient of $R = 0.65$ and a Root Mean Square Error (RMSE) = 0.02 (Figure 5). It should be noted that this agreement is only valid for the location of the soil moisture probes, which is characterized by bare soil and sparse vegetation.

In general, the majority of the in situ soil moisture values range between 0.05 m^3/m^3 and 0.15 m^3/m^3. The SAR-derived SurfMI varies between 20% and 100% relative moisture. The overall agreement between the in situ and satellite-based moisture information implies that the Sentinel-1-derived SurfMI is capable of detecting surface moisture and dynamics.

Figure 6 is showing the averaged time series of the in situ probes and the Sentinel-1-derived surface moisture information. Similar to Figure 5, the Sentinel-1 index is based on an average value per time step for a 3-by-3 pixel area covering the in situ measurements. The in situ soil moisture values represent daily averages and have been converted to relative moisture values for the observation period. The horizontal lines delineates the wet and dry season, which are defined from May to October (dry), and November to April (wet) in each year [10]. In general, the temporal dynamics of the in situ soil moisture values are well represented by the SurfMI, with a mean absolute relative error of 22.5% for the observed period.
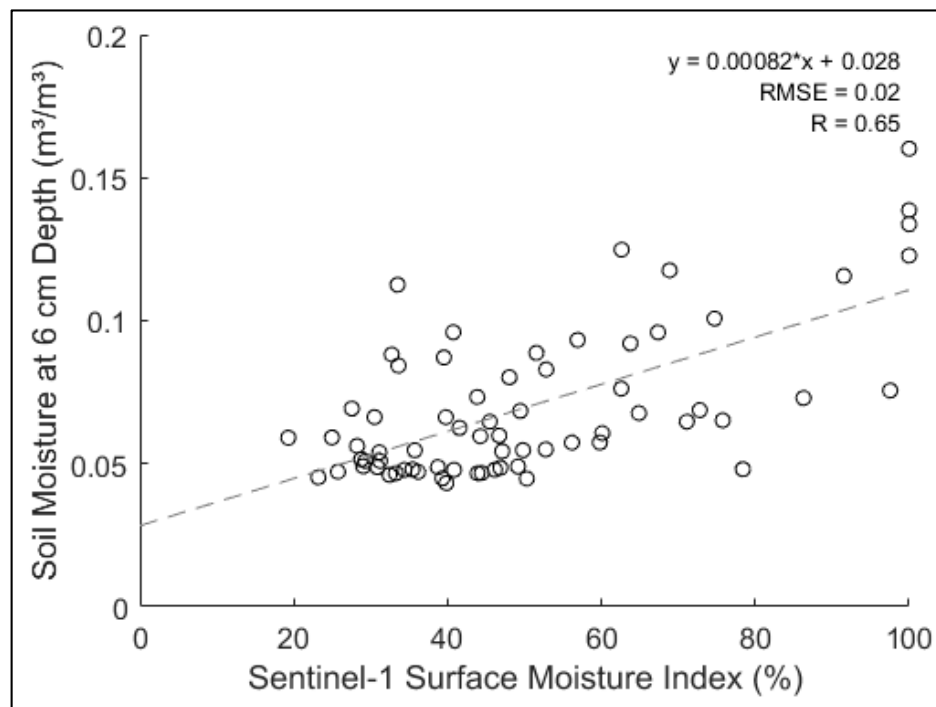
Figure 5. Comparison of in situ soil moisture information and the Sentinel-1-derived surface moisture index (SurfMI) ($N = 69$). The regression line is shown in dashed grey. * is a multiplication symbol.
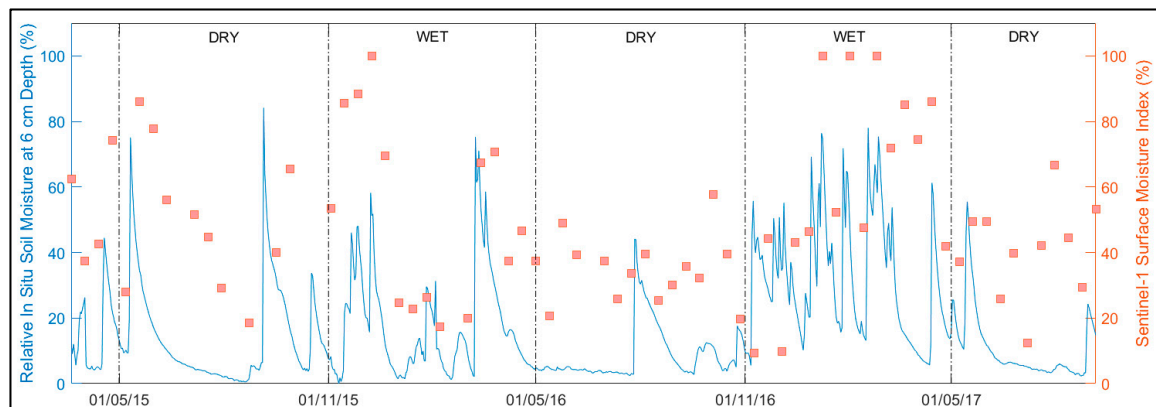

Figure 6. Relative in situ soil moisture information (blue line) and Sentinel-1-derived SurfMI (red dots) time series for the dry (May to October) and wet (November to April) seasons between 2015 and 2017.

The abrupt changes (peaks) in soil moisture content in the upper 6 cm of the soil layer, caused by infiltration after precipitation events, are fairly well covered by the C-band radar-based moisture index (Figure 6). It needs to be highlighted that the moisture content at 6 cm depth is also influenced by a temporal delay as a result of time and intensity of the rain event, the infiltration capacity of the soil, and the time of measurement [66,67]. In addition, small rainfall events may not infiltrate to 6 cm into the soil, yet may influence the SurfMI estimate.

Comparing both wet seasons, only a few abrupt changes in soil moisture are found for the season 2015/2016, whereas the wet season in 2016/2017 is characterized by multiple and more intense changes in soil moisture content at 6 cm depth. The dry seasons of the observed period show only one peak in soil moisture.

Furthermore, decrease in moisture is well captured by the algorithm, which is visible in the dry season of 2015. The decrease of the SurfMI after a precipitation event shows a temporal delay, whereas the in situ measurements show immediate response to the dry-out. However, a time lag in

the radar-derived SurfMI could also be caused by additional moisture input to the uppermost surface layer, which does not have the capacity to infiltrate to 6 cm depth, leading to surface runoff.

The algorithm used for extracting surface moisture dynamics from Sentinel-1 data is also sensitive to small changes in moisture, as found during the wet season of 2015/2016, which has been exceptionally dry with only small precipitation events in the mid-term of the season.

At the location of the in situ soil moisture probes, a CHM derived from a TLS campaign in September 2015 is available. The TLS-derived height information was converted to three land cover classes (ground ≤ 0.5 m, shrub = 0.5–2 m, trees ≥ 2 m) with a spatial resolution of 10 m, in order to compare to the Sentinel-1 data. Based on these classes, individual pixels were selected, representing homogenous areas close to the in situ soil moisture probes. Each of the three clusters contain less than ten pixels. Our aim was to describe the different soil moisture dynamics for different land cover units close to the in situ soil moisture probes. As the TLS dataset is spatially limited to the flux tower location (50 ha), the transfer to larger areas, using Sentinel-2- and Landsat-8-derived vegetation information, is part of the next section.

Figure 7 shows the time series of the Sentinel-1-derived SurfMI for the three different land cover classes, Sentinel-1 cross-polarized (vertical-horizontal—VH) backscatter, which represents the volumetric scattering component of the signal (vegetation structure), as well as precipitation records for this area, which are combined from two stations within the study area.
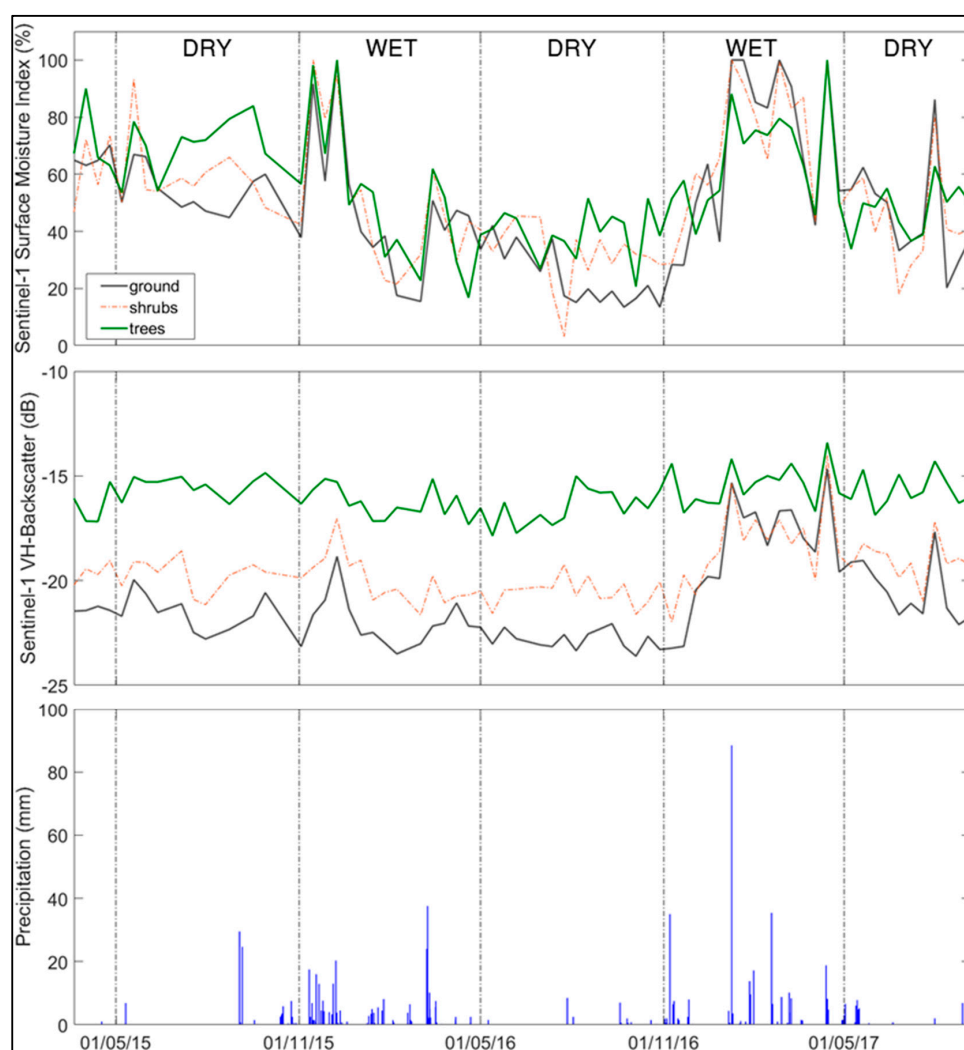

Figure 7. Time series of the Sentinel-1-derived SurfMI (**top**), Sentinel-1 VH backscatter information (dB) for the land cover classes trees, shrubs and ground (**middle**) as well as precipitation records (**bottom**).

During the dry season of 2015, a decline in moisture for the classes shrub and ground was observed. In contrast to that, the tree cover class shows a slight increase in the SurfMI, which is likely related to the fact that the roots can access water and nutrients from deeper soil layers, which are not reachable by shrubs, or used larger stored reserves. The beginning of the wet season in 2015/2016, the exceptional drought period [1,2], is characterized by few and small precipitation events causing an increase in moisture index and volume scattering from vegetation, which was identified in the Senintel-1 VH backscatter time series. The development of grasses on the ground is also influencing the VH backscatter. Since the beginning of 2016, no significant rainfall occurred besides a single precipitation event (around 40 mm). This causes a strong declining trend in the moisture index of the majority of land cover classes during the rest of the wet season as well as the entire dry season in 2016. The dry period leads to an additional decrease in surface moisture for all classes, where bare ground shows larger decrease when compared to shrub and tree cover. Large amounts of precipitation at the beginning of the wet season 2016/2017 resulted in strong increasing trends in the moisture index for the entire season. Comparing both wet seasons, a large difference can be seen in terms of dynamics in moisture regimes as well as vegetation development, characterized by the increase in volume scattering indicated by the C-band VH backscatter. The exceptional drought, which covers the wet and dry seasons in 2015/2016, is characterized by relatively low and decreasing trend in the SurfMI for all classes, which is clearly visible in the Sentinel-1 time series data.

4.2. Drought Impacts on Vegetation Greenness

To analyze the impact of the drought on vegetation greenness, NDVI time series information from Sentinel-2 and Landsat-8 was utilized. Figure 8 shows the combined NDVI time series derived from cloud-free Sentinel-2 and Landsat-8 scenes available for the entire study area within the observed period. Note, that the first Sentinel-2 cloud-free image for this region was available on 26 November 2015. The data coverage during the wet seasons of 2015/2016 and 2016/2017 is limited due to cloud coverage during the rainy season.
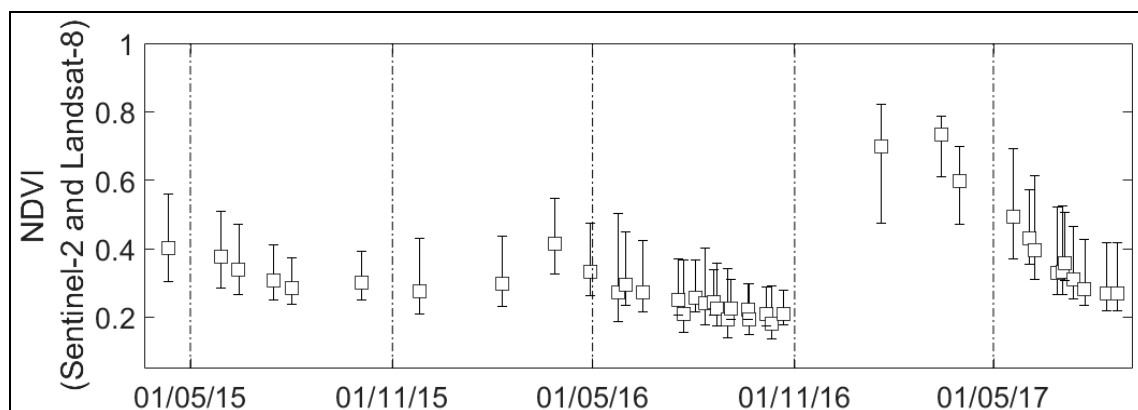

Figure 8. NDVI box plots of time series derived from Sentinel-2 and Landsat-8 for the entire study area.

The impact of the drought on vegetation greenness in late 2015 becomes clearly visible comparing both wet seasons. The difference in average NDVI values between the wet seasons are approximately 0.3 to 0.4. The NDVI values during the dry period are ranging between 0.2 and 0.4, which is almost identical to the wet season of 2015/2016, which indicates very dry conditions with low cover of green vegetation. The wet season of 2016/2017 exhibited high values above an NDVI of 0.6/0.7. The decrease in NDVI values at the beginning of the dry season is significant. This is due to the fact that the region was characterized by high NDVI values during the previous wet season, and reflects the normal senescence of leaves during the dry season.

Figure 9 shows the ΔNDVI, which defines the difference between the NDVI at the start and the end of the wet and dry season, respectively. The dry season of 2015 is dominated by low negative

NDVI changes (approx. −0.1) between start and end of the season. The wet season 2015/2016 is showing a slight increase (approx. 0.1) during this period. Overall, the dry season of 2015 and 2016 are comparable in terms of vegetation greenness. However, during this time, individual trees show a high decline in NDVI, which is likely caused by the loss of tree leaves due to the long-lasting drought with no precipitation for almost one year. By contrast, the wet season of 2016/2017 is characterized by an exceptional increase in NDVI (approx. 0.4). This phenomenon is caused by the occurrence of precipitation during the entire season, resulting in an immediate response of the vegetation. Based on this, the decline in vegetation greening in the follow up season (dry season 2017) is larger compared to the other dry periods.

In general, using Sentinel-2 and Landsat-8 NDVI time series, the impact of the drought from 2015/2016 is clearly visible by the comparison of changes in the NDVI signal, which describes the vegetation greenness and vitality, from the beginning and end of the respective season.
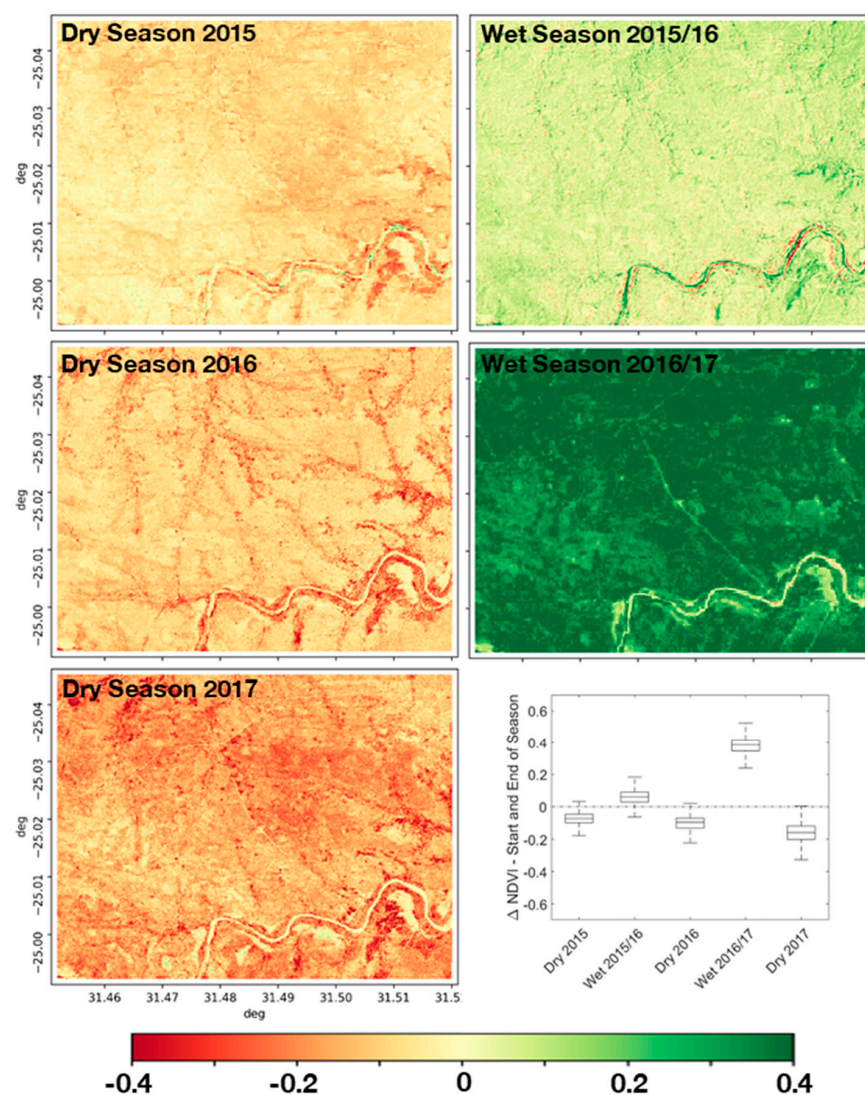

Figure 9. Overview of the ΔNDVI representing the difference between the start and end of each wet and dry season for the entire study area.

4.3. Drought Impacts to Surface Moisture Dependencies of Vegetation Cover

In contrast to Section 4.1, where vegetation information was extracted for a very limited area covered by the TLS data, this section highlights the results analyzing the Sentinel-1-derived SurfMI for larger regions of the study area (see Section 2) by using image objects, which are describing

homogenous land cover types using NDVI time series from Sentinel-2 and Landsat-8. The aim was to focus on a larger scale to analyze the potential of using Sentinel-1 in combination with vegetation information derived from optical Earth observation data (Sentinel-2 and Landsat-8) in order to monitor the impact of droughts in the whole savanna ecosystem.

The object classes distinguish between different vegetation cover (e.g., closed (>60%), open (20–60%), and sparse (<20%), as defined by Gregorio & Jansen [65]), which are comparable to the TLS classes used in Section 4.1. Figure 10 presents the Sentinel-1 derived SurfMI and the Sentinel-1 derived VH backscatter time series for each land cover class, as well as the NDVI time series and the precipitation records. The colored areas around the solid lines display the standard deviation of values inside the corresponding objects.
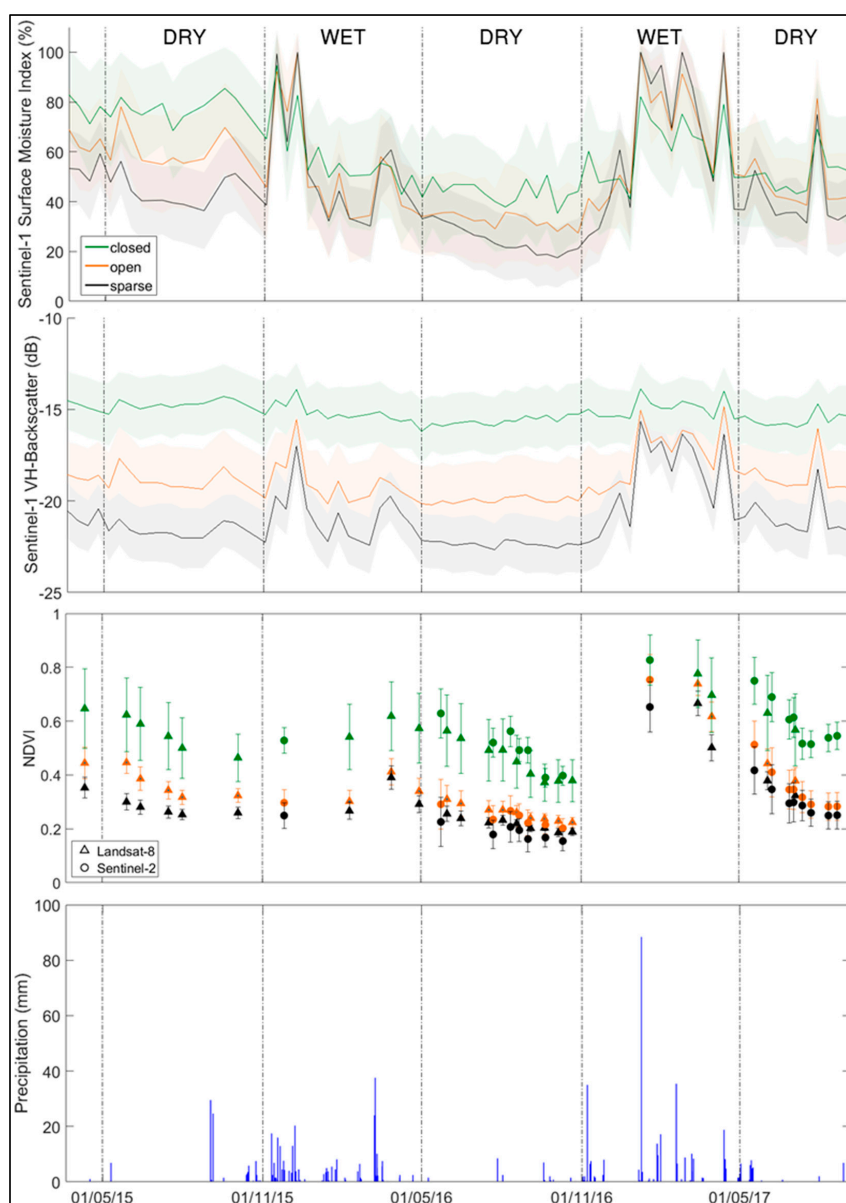

Figure 10. Time series of Sentinel-1 derived moisture index (in %), Sentinel-1 VH backscatter information in dB, NDVI time series derived from Sentinel-2 and Landsat-8, for different land cover units derived by image object segmentation and precipitation in mm records (from top to bottom).

A slight decrease in both the Sentinel-1-derived SurfMI and the NDVI time series are clearly visible during the wet season of 2015 for all three classes. At the same time, the Sentinel-1 VH

backscatter is stable with some exceptions due to small precipitation events towards the end of the season. The wet season from 2015/2016, i.e., the onset of the extraordinary drought, is showing two significant increases in the SurfMI for all classes, which is potentially caused by small precipitation events at the beginning of the wet seasons. The Sentinel-1 VH backscatter time series also shows similar dynamics for the land cover classes "open" and "sparse vegetation". However, the class "closed vegetation" is showing almost no changes in the volumetric scattering processes. As the wet season 2015/2016 was characterized by low amounts of rainfall, it exhibits relatively stable conditions for the NDVI signal describing the vegetation greenness and vitality. The dry season of 2016 featured an additional decline in the SurfMI. Especially the class "sparse vegetation", which is including the majority of bare soil areas, is influenced by these exceptionally dry conditions. The NDVI time series has a very dense temporal resolution as the cloud cover during this period is quite limited. All land cover classes are showing a decreasing NDVI trend. In this time, the decrease in the classes "open" and "sparse vegetation" had the largest decline in NDVI from the end of the wet season. In addition, the SurfMI derived from Sentinel-1 shows a larger impact of drought on low and medium vegetation cover than on closed vegetation cover, dominated by trees [68]. After the extremely dry period from 2015 to 2016, the wet season of 2016/2017 is characterized by a strong precipitation events right at the beginning of the period (refer to Section 4.2). This results in a strong increase in the SurfMI during the entire season. When analyzing the SurfMI, as well as the Sentinel-1 VH backscatter time series, this effect tends to be higher for the land cover classes "open" and "sparse vegetation". After the strong precipitation events, the NDVI values are showing a strong increase for all land cover classes. Unfortunately, no NDVI information was available for the beginning of this particular wet season of 2016/2017, which would potentially allow for a better description of the NDVI time series dynamics. The following dry season experienced almost no significant rain events, which is also clearly visible in the SurfMI and NDVI time series for all observed land cover classes. However, small precipitation events at the beginning of the dry season seem to have a larger impact on the class "sparse vegetation" than on "closed" and "open" vegetation cover types.

5. Discussion

This study focused on the extraction of surface moisture information from high spatial resolution Sentinel-1 time series between 2015 and 2017, using a change detection technique for drought monitoring in combination with NDVI-derived vegetation characteristics from Sentinel-2 and Landsat-8 for a test site in the savanna ecosystem of the southern part of the Kruger National Park.

The comparison of the Sentinel-1 C-band-derived SurfMI to two soil moisture probes shows a good agreement ($R = 0.65$, RMSE = 0.02). The best fit to the regression line was found for the SurfMI range between 20% and 60% (Figure 5), which corresponds to the findings of [69]. It needs to be mentioned that the availability of additional ground-based soil moisture information is sparse in this study area. Supplementary in situ information from other areas within the study area would facilitate an enhanced analysis of the agreement between the remote sensing-derived and ground-based moisture measurements. However, the overall agreement between the measurements has shown that the derived SurfMI is a suitable tool for drought monitoring using high spatial Earth observation data.

Various aspects affect the comparison of satellite-derived moisture information with ground-based measurements. Large amounts of rainfall during the image acquisition might introduce significant uncertainties when comparing satellite-derived surface moisture to in situ soil moisture, as water is likely to be present at the surface, influencing the backscatter signal. In our time series, we found that seven out of 69 observations have been acquired when a precipitation event took place during the same day. However, as the rain intensity was very low on these dates (less than 2 mm on average), and as we compared the SAR-based surface moisture information to daily in situ averages only, this circumstance can be neglected. In addition, soil infiltration processes and timing are influenced by different factors, such as soil type, soil temperature, existing moisture content, evaporation potential, surface roughness, etc. [39,61,67]. However, a drying of the upper surface layer, which is detected by

the satellite signal, might not be visible in the in situ measurements, which are acquired 6 cm below the ground, thus causing an additional source of uncertainty.

The seasonal variations and short-term changes in the in situ soil moisture time series have been well represented by the Sentinel-1-derived SurfMI. This sensitivity was especially found during the wet season of 2015/2016, which was classified as an exceptional drought period as only a few precipitation events in the mid-term of the wet season with low amounts of rainfall were recorded. The utilization of Sentinel-1A and -1B, which will enhance the temporal resolution of the time series by increasing the repetition rate to approximately six days, is likely to even further improve the representation of small-term moisture changes by the SAR-based change detection approach.

Moisture variability and dynamics for different vegetation cover classes in the observed period have been analyzed by the integration of Sentinel-2 and Landsat-8 time series information (Figure 10). During the wet season of 2015/2016, all vegetation cover classes are exhibiting a similar declining response in the Sentinel-1-derived SurfMI, due to the absence of precipitation. In particular, open and sparsely vegetated areas are showing large declines. The subsequent dry period, which is also characterized by extremely low precipitation rates, is indicating the strongest decline in the SurfMI for non-vegetated areas, whereas vegetated areas are characterized by more stable conditions in the SurfMI. The end of this drought period (wet season 2016/2017) coincided with large precipitation events at the beginning of the season, and resulted in a sharp increase in the Sentinel-1 moisture index for all observed vegetation classes (close, open, and sparse). However, open and sparsely vegetated areas feature a much larger increase in the SurfMI. Further, the NDVI time series from Sentinel-2 and Landsat-8 are showing a similar response as the surface moisture observations. The class "closed vegetation" showed a more stable NDVI signal than the classes "open" and "sparse", which were also visible during the rainy period where those classes were characterized by greater variations. These findings are comparable to the study of Berry et al. [70], which showed that even precipitation events of low intensity are increasing the water availability of the root system of the woody vegetation (below 20 cm soil depth), whereas the development of grasses is directly linked to precipitation events and the water availability in the upper 20 cm. Thus, an increase in woody vegetation biomass in periods of less precipitation is possible, as tree roots reach deeper soil layers with remaining water content, making use of stored reserves. These circumstances are visualized in Figure 9, where the ΔNDVI indicates remaining vegetation greenness of larger tree communities, which are situated in the riparian areas of a tributary of the Sabie River in the southern part of the study area during the drought period of 2015/2016. Hence, analyzing surface moisture information from high-resolution Sentinel-1 C-band time series data in savanna ecosystems requires detailed information on existing vegetation cover and phenology. Besides the used change detection methodology for the surface moisture retrieval, future investigations might also focus on utilizing additional approaches, such as the artificial neural network and water cloud models, which are widely used for the extraction of soil moisture information from optical and SAR Earth observation data. These approaches are showing promising results, but require additional in situ information for training and testing of the modelling, which is limited to large scale surface moisture monitoring [46].

As the ENSO phenomenon has potentially intensified during the last century [71,72], it is likely that extreme drought events in South Africa will happen more frequently, as well as in increased strength and duration. The so called "flash drought phenomenon", which is characterized by scarcity of soil moisture in combination with extremely high air temperatures (e.g., heat waves) [73,74], has already increased by 220% in South Africa during the last 50 years, and is mainly attributed to anthropogenic climate change [75]. This phenomenon will introduce vast changes to savanna ecosystems in the future, which requires adaption of economic and natural management structures in order to prevent drought-induced impacts to humans and nature, such as food shortage, water scarcity, wildfires, etc. To overcome this problem, new state-of-the-art and innovative forecast applications and tools, operating with high spatial and temporal resolution information from recent satellite missions, are essential requirements [76]. In addition to monitoring the spatiotemporal extent of droughts under

a changing climate regime, large scale surface moisture estimates, as presented here, could also prove valuable for landscape management. For example, fuel moisture, climatic variables (e.g., wind speed and relative humidity), and fuel loads, are critical variables with which to estimate fire risk, behavior, and intensity [77]. Expanding the work presented here to allow for accurate and timely estimates of fuel moisture over large landscapes will, in combination with other remote sensing products (e.g., fuel loads; [78]), provide valuable tools for managers in fire-prone ecosystems to predict areas at risk of fire and, possibly, tools with which to estimate fire intensity.

6. Conclusions

The objective of this paper was to derive surface moisture information from Sentinel-1 C-band time series data for drought monitoring for a selected test area in the southern part of the KNP, South Africa. In addition, multi-temporal Sentinel-2 and Landsat-8 NDVI information was derived to compare the findings from the SAR-based SurfMI to different vegetation cover types and their phenological dynamics. The analysis was carried out for the time period between March 2015 and November 2017, including one of the most severe drought events in South Africa (2015/2016) since climate recordings began.

We found good agreement ($R = 0.65$, RMSE = 0.02) between the SurfMI, derived from VV-polarized Sentinel-1 time series information, with in situ soil moisture values recorded near the Skukuza flux tower. The dynamics of the temporal profiles are matching very well when comparing the SAR-based moisture index with in situ soil moisture information. In addition, even small changes in moisture regimes were detected by Sentinel-1, which indicates the suitability of utilizing the data for drought monitoring. Deriving different moisture time series profiles for different vegetation units, which were based on a TLS classification, we found that vegetated areas exhibit a time lag in reaction to moisture changes, e.g., stronger decline in moisture for ground areas during dry-out phases. As the vegetation information from TLS is only limited to a very small area, we used Sentinel-2 and Landsat-8 NDVI data to compare the SurfMI from Sentinel-1 for different vegetation cover classes based on the Food and Agriculture Organization of the United Nations—Land Cover Classification System on larger scale. Using larger areas, the impact of the drought in the southern summer of 2015/2016 is clearly visible. However, vegetation areas including tree and shrub cover showed different reactions between the precipitation events and dry-out phases when compared to bare ground, which indicates an immediate response to changes in moisture regimes.

We conclude that it is of high importance to use land cover and vegetation information for analyzing surface moisture dynamics derived by Earth observation time series. The knowledge on vegetation cover, as well as the phenology, is central to the development of a drought monitoring system for savanna ecosystems.

References

1. RIASCO (Regional Interagency Standing Committee). Response Plan for the El Niño-Induced Drought in Southern Africa. 2016. Available online: https://reliefweb.int/report/world/riasco-action-plan-southern-africa-response-plan-el-ni-o-induced-drought-southern (accessed on 14 September 2018).

2. Liberto, T. Di A Not so Rainy Season: Drought in Southern Africa in January 2016. Available online: https://www.climate.gov/news-features/event-tracker/not-so-rainy-season-drought-southern-africa-january-2016 (accessed on 25 April 2018).

3. Singels, A.; Potgieter, A.B. A technique to evaluate ENSO-based maize production strategies. *S. Afr. J. Plant Soil* **1997**, *14*, 93–97. [CrossRef]

4. Malherbe, J.; Dieppois, B.; Maluleke, P.; Van Staden, M.; Pillay, D.L. South African droughts and decadal variability. *Nat. Hazards* **2016**, *80*, 657–681. [CrossRef]

5. Magrath, J. *Entering Uncharted Waters: El Niño and the Threat to Food Security*; Oxfam International: Oxfam, UK, 2015.

6. Cane, M.A.; Eshel, G.; Buckland, R.W. Forecasting Zimbabwean maize yield using eastern equatorial Pacific sea surface temperature. *Nature* **1994**, *370*, 204–205. [CrossRef]

7. Anyamba, A.; Tucker, C.J.; Mahoney, R. From El Niño to La Niña: Vegetation Response Patterns over East and Southern Africa during the 1997–2000 Period. *J. Clim.* **2002**, *15*, 3096–3103. [CrossRef]

8. Trenberth, K.E.; Stepaniak, D.P. Indices of El Niño evolution. *J. Clim.* **2001**, *14*, 1697–1701. [CrossRef]

9. Masih, I.; Maskey, S.; Mussá, F.E.F.; Trambauer, P. A review of droughts on the African continent: A geospatial and long-term perspective. *Hydrol. Earth Syst. Sci.* **2014**, *18*, 3635–3649. [CrossRef]

10. Rouault, M.; Richard, Y. Intensity and spatial extension of drought in South Africa at different time scales. *Water SA* **2003**, *29*, 489–500. [CrossRef]

11. Eberle, J.; Clausnitzer, S.; Hüttich, C.; Schmullius, C. Multi-Source Data Processing Middleware for Land Monitoring within a Web-Based Spatial Data Infrastructure for Siberia. *ISPRS Int. J. Geo-Inf.* **2013**, *2*, 553–576. [CrossRef]

12. NOAA. NOAA's Climate Prediction Center. Available online: http://origin.cpc.ncep.noaa.gov/products/analysis_monitoring/ensostuff/ONI_v5.php (accessed on 28 November 2017).

13. Kutsch, W.; Hanan, N.; Scholes, B.; McHugh, I.; Kubheka, W.; Eckhardt, H.; Williams, C. Response of carbon fluxes to water relations in a savanna ecosystem in South Africa. *Biogeosciences* **2008**, *5*, 1797–1808. [CrossRef]

14. Main, R.; Mathieu, R.; Kleynhans, W.; Wessels, K.; Naidoo, L.; Asner, G.P. Hyper-temporal C-band SAR for baseline woody structural assessments in deciduous savannas. *Remote Sens.* **2016**, *8*, 661. [CrossRef]

15. Scholes, R.J.; Archer, S.R. Tree-Grass Interactions in Savannas. *Annu. Rev. Ecol. Syst.* **1997**, *28*, 517–544. [CrossRef]

16. Druce, D.J.; Shannon, G.; Page, B.R.; Grant, R.; Slotow, R. Ecological thresholds in the Savanna landscape: Developing a protocol for monitoring the change in composition and utilisation of large trees. *PLoS ONE* **2008**, *3*, e3979. [CrossRef] [PubMed]

17. Hill, M.J. Vegetation index suites as indicators of vegetation state in grassland and savanna: An analysis with simulated SENTINEL 2 data for a North American transect. *Remote Sens. Environ.* **2013**, *137*, 94–111. [CrossRef]

18. Archibald, S.; Scholes, R.J. Leaf green-up in a semi-arid African savanna - separating tree and grass responses to environmental cues. *J. Veg. Sci.* **2007**, *18*, 583–594. [CrossRef]

19. Grant, R.C.C.; Peel, M.J.S.; Bezuidenhout, H. Evaluating herbivore management outcomes and associated vegetation impacts. *Koedoe* **2011**, *53*, 1–15. [CrossRef]

20. AghaKouchak, A.; Farahmand, A.; Melton, F.S.; Teixeira, J.; Anderson, M.C.; Wardlow, B.D.; Hain, C.R. Remote sensing of drought: Progress, challenges and opportunities. *Rev. Geophys.* **2015**, *53*, 452–480. [CrossRef]

21. Bijaber, N.; El Hadani, D.; Saidi, M.; Svoboda, M.; Wardlow, B.; Hain, C.; Poulsen, C.; Yessef, M.; Rochdi, A. Developing a Remotely Sensed Drought Monitoring Indicator for Morocco. *Geosciences* **2018**, *8*, 55. [CrossRef]

22. Zeng, L.; Shan, J.; Xiang, D. Monitoring drought using multi-sensor remote sensing data in cropland of Gansu Province. In *IOP Conference Series: Earth and Environmental Science*; IOP Publishing: Bristol, UK, 2014; Volume 17.

23. Villarreal, M.L.; Norman, L.M.; Buckley, S.; Wallace, C.S.A.; Coe, M.A. Multi-index time series monitoring of drought and fire effects on desert grasslands. *Remote Sens. Environ.* **2016**, *183*, 186–197. [CrossRef]

24. He, B.; Liao, Z.; Quan, X.; Li, X.; Hu, J. A global Grassland Drought Index (GDI) product: Algorithm and validation. *Remote Sens.* **2015**, *7*, 12704–12736. [CrossRef]

25. Western, D.; Mose, V.N.; Worden, J.; Maitumo, D. Predicting Extreme Droughts in Savannah Africa: A Comparison of Proxy and Direct Measures in Detecting Biomass Fluctuations, Trends and Their Causes. *PLoS ONE* **2015**, *10*, e0136516. [CrossRef]

26. Graw, V.; Ghazaryan, G.; Dall, K.; Gómez, A.D.; Abdel-Hamid, A.; Jordaan, A.; Piroska, R.; Post, J.; Szarzynski, J.; Walz, Y.; et al. Drought dynamics and vegetation productivity in different land management systems of Eastern Cape, South Africa—A remote sensing perspective. *Sustainability* **2017**, *9*, 1728. [CrossRef]

27. Makhado, R.A.; Scholes, R.J. Determinants of soil respiration in a semi-arid savanna ecosystem, Kruger National Park, South Africa. *Koedoe* **2011**, *53*, 1–8. [CrossRef]

28. Entekhabi, D.; Njoku, E.G.; O'Neill, P.E.; Kellogg, K.H.; Crow, W.T.; Edelstein, W.N.; Entin, J.K.; Goodman, S.D.; Jackson, T.J.; Johnson, J.; et al. The Soil Moisture Active Passive (SMAP) Mission. *Proc. IEEE* **2010**, *98*, 704–716. [CrossRef]

29. Kerr, Y.H.; Waldteufel, P.; Richaume, P.; Wigneron, J.P.; Ferrazzoli, P.; Mahmoodi, A.; Al Bitar, A.; Cabot, F.; Gruhier, C.; Juglea, S.E.; et al. The SMOS soil moisture retrieval algorithm. *IEEE Trans. Geosci. Remote Sens.* **2012**, *50*, 1384–1403. [CrossRef]

30. Altese, E.; Bolognani, O.; Mancini, M.; Troch, P.A. Retrieving soil moisture over bare soil from ERS 1 synthetic aperture radar data: Sensitivity analysis based on a theoretical surface scattering model and field data. *Water Resour. Res.* **1996**, *32*, 653–661. [CrossRef]

31. Bourgeau-Chavez, L.L.; Kasischke, E.S.; Riordan, K.; Brunzell, S.; Nolan, M.; Hyer, E.; Slawski, J.; Medvecz, M.; Walters, T.; Ames, S. Remote monitoring of spatial and temporal surface soil moisture in fire disturbed boreal forest ecosystems with ERS SAR imagery. *Int. J. Remote Sens.* **2007**, *28*, 2133–2162. [CrossRef]

32. Haider, S.S.; Said, S.; Kothyari, U.C.; Arora, M.K. Soil moisture estimation using ERS 2 SAR data: A case study in the Solani River catchment/Estimation de l'humidité du sol grâce à des données ERS-2 SAR: Étude de cas dans le bassin de la rivière Solani. *Hydrol. Sci. J.* **2004**, *49*, 334. [CrossRef]

33. Holah, N.; Baghdadi, N.; Zribi, M.; Bruand, A.; King, C. Potential of ASAR/ENVISAT for the characterization of soil surface parameters over bare agricultural fields. *Remote Sens. Environ.* **2005**, *96*, 78–86. [CrossRef]

34. Zribi, M.; Baghdadi, N.; Holah, N.; Fafin, O. New methodology for soil surface moisture estimation and its application to ENVISAT-ASAR multi-incidence data inversion. *Remote Sens. Environ.* **2005**, *96*, 485–496. [CrossRef]

35. Paloscia, S.; Pampaloni, P.; Pettinato, S.; Santi, E. A comparison of algorithms for retrieving soil moisture from ENVISAT ASAR images. *IEEE Trans. Geosci. Remote Sens.* **2008**, *46*, 3274–3284. [CrossRef]

36. Biftu, G.F.; Gan, T.Y. Retrieving near-surface soil moisture from Radarsat SAR data. *Water Resour. Res.* **1999**, *35*, 1569–1579. [CrossRef]

37. Leconte, R.; Brissette, F.; Galarneau, M.; Rousselle, J. Mapping near-surface soil moisture with RADARSAT-1 synthetic aperture radar data. *Water Resour. Res.* **2004**, *40*. [CrossRef]

38. Glenn, N.F.; Carr, J.R. Establishing a relationship between soil moisture and RADARSAT-1 SAR data obtained over the Great Basin, Nevada, USA. *Can. J. Remote Sens.* **2004**, *30*, 176–181. [CrossRef]

39. Mohanty, B.P.; Cosh, M.H.; Lakshmi, V.; Montzka, C. Soil Moisture Remote Sensing: State-of-the-Science. *Vadose Zone J.* **2017**, *16*. [CrossRef]

40. Paloscia, S.; Pettinato, S.; Santi, E.; Notarnicola, C.; Pasolli, L.; Reppucci, A. Soil moisture mapping using Sentinel-1 images: Algorithm and preliminary validation. *Remote Sens. Environ.* **2013**, *134*, 234–248. [CrossRef]

41. Wagner, W.; Sabel, D.; Doubkova, M.; Bartsch, A.; Pathe, C. The Potential of Sentinel-1 for Monitoring Soil Moisture With a High Spatial Resolution At Global Scale. *Earth Obs. Water Cycle Sci.* **2009**, *2009*, 18–20.

42. Garkusha, I.N.; Hnatushenko, V.V.; Vasyliev, V.V. Using Sentinel-1 data for monitoring of soil moisture. In Proceedings of the 2017 IEEE International Geoscience and Remote Sensing Symposium (IGARSS), Fort Worth, TX, USA, 23–28 July 2017; pp. 6–9.

43. Lievens, H.; Reichle, R.H.; Liu, Q.; De Lannoy, G.J.M.; Dunbar, R.S.; Kim, S.B.; Das, N.N.; Cosh, M.; Walker, J.P.; Wagner, W. Joint Sentinel-1 and SMAP data assimilation to improve soil moisture estimates. *Geophys. Res. Lett.* **2017**, *44*, 6145–6153. [CrossRef] [PubMed]

44. Alexakis, D.D.; Mexis, F.D.K.; Vozinaki, A.E.K.; Daliakopoulos, I.N.; Tsanis, I.K. Soil moisture content estimation based on Sentinel-1 and auxiliary earth observation products. A hydrological approach. *Sensors* **2017**, *17*, 1455. [CrossRef] [PubMed]

45. Cenci, L.; Pulvirenti, L.; Boni, G.; Chini, M.; Matgen, P.; Gabellani, S.; Squicciarino, G.; Pierdicca, N. An evaluation of the potential of Sentinel 1 for improving flash flood predictions via soil moisture-data assimilation. *Adv. Geosci.* **2017**, *44*, 89–100. [CrossRef]

46. Gao, Q.; Zribi, M.; Escorihuela, M.J.; Baghdadi, N. Synergetic use of Sentinel-1 and Sentinel-2 data for soil moisture mapping at 100 m resolution. *Sensors* **2017**, *17*, 1966. [CrossRef] [PubMed]

47. Naeimi, V.; Scipal, K.; Bartalis, Z.; Hasenauer, S.; Wagner, W. An improved soil moisture retrieval algorithm for ERS and METOP scatterometer observations. *IEEE Trans. Geosci. Remote Sens.* **2009**, *47*, 1999–2013. [CrossRef]

48. Wagner, W.; Lemoine, G.; Rott, H. A method for estimating soil moisture from ERS Scatterometer and soil data. *Remote Sens. Environ.* **1999**, *70*, 191–207. [CrossRef]

49. Lenfers, U.A.; Bruggemann, R.; Clemen, T. Exploring survival strategies of African Savanna trees by partial ordering techniques. *Ecol. Inform.* **2017**, *42*, 14–23. [CrossRef]

50. Colgan, M.S.; Asner, G.P.; Levick, S.R.; Martin, R.E.; Chadwick, O.A. Topo-edaphic controls over woody plant biomass in South African savannas. *Biogeosciences* **2012**, *9*, 1809–1821. [CrossRef]

51. Venter, F.J.; Scholes, R.J.; Eckhardt, H.; du Toit, R. The abiotic template and its associated vegetation pattern. In *The Kruger Experience: Ecology and Management of Savanna Heterogeneity*; Du Toit, R., Biggs, H.C., Rogers, K.H., Eds.; Island Press: Washington, DC, USA, 2003; pp. 83–129.

52. Truckenbrodt, J. pyroSAR—A Python Framework for Large-Scale SAR Satellite Data Processing. Available online: https://github.com/johntruckenbrodt/pyroSAR (accessed on 29 November 2017).

53. Wegmüller, U.; Werner, C.; Strozzi, T.; Wiesmann, A.; Frey, O.; Santoro, M. Sentinel-1 Support in the GAMMA Software. *Procedia Comput. Sci.* **2016**, *100*, 1305–1312. [CrossRef]

54. USGS (United States Geological Survey). *Shuttle Radar Topography Mission (SRTM) 1 Arc-Second Global—Version 3*; USGS: Reston, VA, USA, 2018.

55. Small, D. Flattening gamma: Radiometric terrain correction for SAR imagery. *IEEE Trans. Geosci. Remote Sens.* **2011**, *49*, 3081–3093. [CrossRef]

56. Louis, J.; Debaecker, V.; Pflug, B.; Main-Knorn, M.; Bieniarz, J.; Mueller-Wilm, U.; Cadau, E.; Gascon, F. Sentinel-2 SEN2COR: L2A processor for users. In *European Space Agency, (Special Publication) ESA SP*; ESA Living Planet Symposium: Praque, Czech Republic, 2016; Volume SP-740.

57. Vermote, E.; Justice, C.; Claverie, M.; Franch, B. Preliminary analysis of the performance of the Landsat 8/OLI land surface reflectance product. *Remote Sens. Environ.* **2016**, *185*, 46–56. [CrossRef]

58. Goosen, L. Kruger National Park Daily Rainfall Data 2012 until Present. Available online: http://dataknp.sanparks.org/sanparks/metacat (accessed on 30 November 2017).

59. Chuvieco, E. *Fundamentals of Satellite Remote Sensing an Environmental Approach*; CRC Press, an imprint of the Taylor & Francis Group: Boca Raton, FL, USA, 2016; ISBN 9781498728096.

60. Odipo, V.; Nickless, A.; Berger, C.; Baade, J.; Urbazaev, M.; Walther, C.; Schmullius, C. Assessment of Aboveground Woody Biomass Dynamics Using Terrestrial Laser Scanner and L-Band ALOS PALSAR Data in South African Savanna. *Forests* **2016**, *7*, 294. [CrossRef]

61. Verstraeten, W.W.; Veroustraete, F.; Van Der Sande, C.J.; Grootaers, I.; Feyen, J. Soil moisture retrieval using thermal inertia, determined with visible and thermal spaceborne data, validated for European forests. *Remote Sens. Environ.* **2006**, *101*, 299–314. [CrossRef]

62. Entekhabi, D.; Njoku, E.G.; Houser, P.; Spencer, M.; Doiron, T.; Kim, Y.; Smith, J.; Girard, R.; Belair, S.; Crow, W.; et al. The hydrosphere state (hydros) satellite mission: An earth system pathfinder for global mapping of soil moisture and land freeze/thaw. *IEEE Trans. Geosci. Remote Sens.* **2004**, *42*, 2184–2195. [CrossRef]

63. Tucker, C.J. Red and photographic infrared linear combinations for monitoring vegetation. *Remote Sens. Environ.* **1979**, *8*, 127–150. [CrossRef]

64. Zhang, H.K.; Roy, D.P.; Yan, L.; Li, Z.; Huang, H.; Vermote, E.; Skakun, S.; Roger, J.C. Characterization of Sentinel-2A and Landsat-8 top of atmosphere, surface, and nadir BRDF adjusted reflectance and NDVI differences. *Remote Sens. Environ.* **2018**, *215*, 482–494. [CrossRef]

65. Di Gregorio, A.; Jansen, L.J.M. *Land Cover Classification System (LCCS): Classification Concepts and User Manual*; Software; FAO: Rome, Italy, 2005.

66. Hillel, D. *Introduction to Environmental Soil Physics*; Elsevier Academic Press: Cambridge, MA, USA, 2003; ISBN 9780123486554.

67. Kirkham, M.B. *Principles of Soil and Plant Water Relations*; Elsevier Academic Press: Cambridge, MA, USA, 2005; ISBN 9780124097513.

68. Nicolai-Shaw, N.; Zscheischler, J.; Hirschi, M.; Gudmundsson, L.; Seneviratne, S.I. A drought event composite analysis using satellite remote-sensing based soil moisture. *Remote Sens. Environ.* **2017**, *203*, 216–225. [CrossRef]

69. Shoshany, M.; Svoray, T.; Svoray, T.; Curran, P.J.; Foody, G.M.; Perevolotsky, A. The relationship between ERS-2 SAR backscatter and soil moisture: Generalization from a humid to semi-arid transect. *Int. J. Remote Sens.* **2000**, *21*, 2337–2343. [CrossRef]

70. Berry, R.S.; Kulmatiski, A. A savanna response to precipitation intensity. *PLoS ONE* **2017**, *12*, e0175402. [CrossRef] [PubMed]

71. Cai, W.; Borlace, S.; Lengaigne, M.; Van Rensch, P.; Collins, M.; Vecchi, G.; Timmermann, A.; Santoso, A.; Mcphaden, M.J.; Wu, L.; et al. Increasing frequency of extreme El Niño events due to greenhouse warming. *Nat. Clim. Chang.* **2014**, *4*, 111–116. [CrossRef]

72. Perry, S.J.; McGregor, S.; Gupta, A.S.; England, M.H. Future Changes to El Niño–Southern Oscillation Temperature and Precipitation Teleconnections. *Geophys. Res. Lett.* **2017**, *44*, 10608–10616. [CrossRef]

73. Hunt, E.D.; Hubbard, K.G.; Wilhite, D.A.; Arkebauer, T.J.; Dutcher, A.L. The development and evaluation of a soil moisture index. *Int. J. Climatol.* **2009**, *29*, 747–759. [CrossRef]

74. Senay, G.B.; Budde, M.B.; Brown, J.F.; Verdin, J.P. Mapping flash drought in the US: Southern Great Plains. In Proceedings of the 22nd Conference on Hydrology, AMS, New Orleans, LA, USA, 20–24 January 2008.

75. Yuan, X.; Wang, L.; Wood, E.F. Anthropogenic Intensification of Southern African Flash Droughts as Exemplified by the 2015/2016 Season. In *Explaining Extreme Events of 2016 from a Climate Perspective*; Herring, S.C., Christidis, N., Hoell, A., Kossin, J.P., Schreck, C.J., III, Stott, P.A., Eds.; Bulletin of the American Meteorological Society: Boston, MA, USA, 2018; Volume 98, pp. S86–S90.

76. Wanders, N.; Wood, E.F. Assessing Seasonal Climate Forecasts Over Africa to Support Decision-Making. In *Bridging Science and Policy Implication for Managing Climate Extremes*; Hong-Sang Jung, B.W., Ed.; World Scientific Publishing Co. Pte. Ltd. and APEC Climate Center: Singapore, 2018; pp. 1–15, ISBN 9789813235663.

77. Byram, G.M. Combustion of forest fuels. In *Forest Fire: Control and Use*; Davis, K.P., Ed.; McGraw-Hill: New York, NY, USA, 1959; pp. 155–182.

78. Wessels, K.J.; Prince, S.D.; Zambatis, N.; MacFadyen, S.; Frost, P.E.; Van Zyl, D. Relationship between herbaceous biomass and 1-km^2 Advanced Very High Resolution Radiometer (AVHRR) NDVI in Kruger National Park, South Africa. *Int. J. Remote Sens.* **2006**, *27*, 951–973. [CrossRef]